ASEG Extended Abstracts

ISSN: 2202-0586 (Print) (Online) Journal homepage: https://www.tandfonline.com/loi/texg19

An AI approach to automated magnetic formation mapping beneath cover

David A. Pratt, K. Blair McKenzie & Anthony S. White

To cite this article: David A. Pratt, K. Blair McKenzie & Anthony S. White (2019) An AI approach to automated magnetic formation mapping beneath cover, ASEG Extended Abstracts, 2019:1, 1-9, DOI: 10.1080/22020586.2019.12073001

To link to this article: https://doi.org/10.1080/22020586.2019.12073001

AEGC2019 Data to Discovery
Australasian Exploration Geoscience Conference
2-5 September 2019 • Perth, Western Australia
Incorporating the AIG, ASEG, PESA, and WABS

An AI approach to automated magnetic formation mapping beneath cover

David A. Pratt*
Tensor Research P/L
PO Box 5189
Greenwich NSW 2065
Australia
david.pratt@tensor-research.com.au

K. Blair McKenzie
Tensor Research P/L
PO Box 5189
Greenwich NSW 2065
Australia
blair.mckenzie@tensor-research.com.au

Anthony S. White
Tensor Research P/L
PO Box 5189
Greenwich NSW 2065
Australia
tony.white@tensor-research.com.au

SUMMARY

Most regional scale magnetic maps are dominated by the magnetic characteristics of steeply dipping basement units truncated by an unconformity surface. It is easy to demonstrate that 80 to 90% of each total field magnetic anomaly is contributed by this intersecting surface. We approach this problem by mapping the boundaries between contrasting magnetic units along each line in the magnetic survey using the full precision of the line data and 3D information from the magnetic gradient tensor. Additionally, we derive the azimuth of each boundary, depth to the unconformity and magnetic properties of the anomalous units. The segments are overlain on any image such as existing geological maps, satellite imagery, gravity or magnetic imagery to provide a new geological interpretation concept. This method provides a new way to interpret new and old magnetic surveys.

Eigenvector analysis of the magnetic tensor and normalised source strength (NSS) are combined with an artificial intelligence (AI) approach to estimate the basement properties. The method is applied to full tensor magnetic survey data or a grid of the total magnetic intensity data is processed using FFT transformations to derive the magnetic gradient tensor. These data are used as input to the pre-trained AI process for calculation of depth, width, azimuth, magnetic susceptibility and magnetisation direction. The rock properties and depth information can be used for 3D visualisation of the unconformity and 2D mapping of the magnetic lithology of the unconformity surface.

Key words: AI, magnetic, tensor, mapping, basement.

INTRODUCTION

An AI approach requires a geological model concept that is well suited to automated interpretation. Our autonomous approach to geological mapping is based on three important concepts:

- the unconformity geological model
- geological attributes of the magnetic tensor
- an AI approach to converting attributes to geology

There are numerous tools available to assist geoscientists with the interpretation of aeromagnetic surveys ranging from specialised enhancement tools to full 3D modelling and inversion of the data. Enhancement methods are generally focussed on differentiating geological units in a 2D sense, while modelling and inversion require an underlying geological model concept to provide appropriate constraints.

We focus on the use of a geologic model to produce a new approach to geological mapping of the basement unconformity surface (Figure 1). This concept was first developed by Pratt et al. (2001) to build a starting 3D model of an isolated magnetic anomaly for seeding a 3D magnetic inversion.

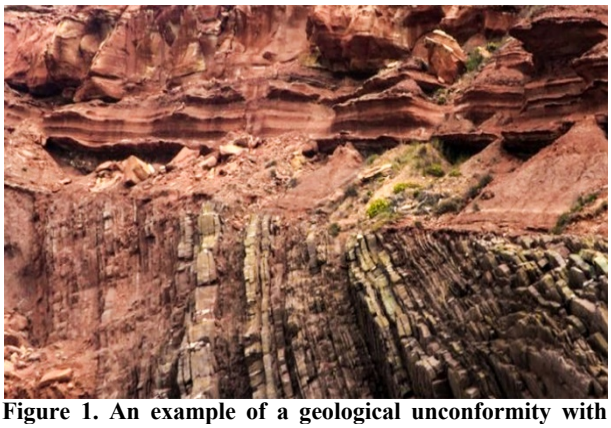

Figure 1. An example of a geological unconformity with steeply dipping basement rocks.

Our understanding of the inherent information that can be derived from the magnetic tensor has extended our original concept to allow autonomous mapping of the unconformity with the aid of AI concepts. We use an expert system, artificial intelligence (AI) methodology for integrating the complex relationships between the quantitative geophysical methods and constraining geological principles (Pratt et al., 2019).

Unconformity Dominance

The dominant influence of the unconformity surface on measured magnetic anomalies is often ignored in large scale voxel inversions. A cursory review of most exploration and regional surveys will show the magnetic images are an excellent proxy for the geology at the unconformity surface. This dominance is illustrated in Figure 2 which shows that more than 90% of the total magnetic intensity anomaly is derived from the unconformity surface, with the remaining 10% distributed between the surface and the Curie point.

The model is a linear magnetic formation extending from the unconformity at 200 metres below the sensor to a depth of 10,000 metres. The base of the model was then raised to depths of 1,000, 500 and 200 metres and then inverted against the original 10,000 metre depth extent model data. The total magnetic intensity curves are shown in the middle track and

the residual difference curves are shown in the top track at the same scale. The RMS difference between each of the models is shown to the left of each model.

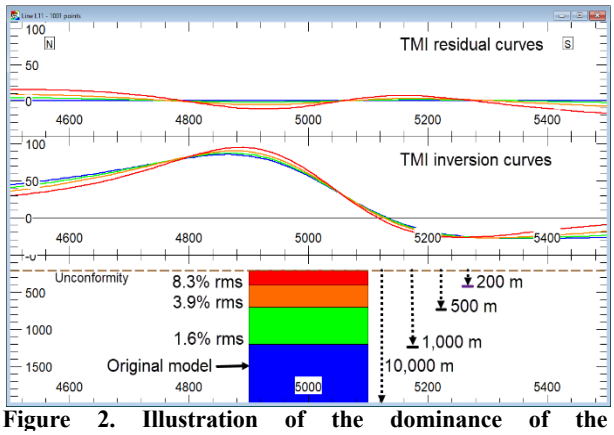

Figure 2. Illustration of the dominance of the unconformity. The four models are 200 m wide, 200 m below the sensor with depth extents of 200 m (red), 500 m (orange), 1000 m (green) and 10 km (blue) below the unconformity. The middle track shows the TMI curve in blue for the 10 km depth extent model and the inverted responses for the other three depth extents. The upper track shows the residual difference curves with rms values of 1.6%, 3.9% and 8.3% for the 1000 m, 500 m and 200 m depth extent models.

The implications of these results are used to support the robustness of the model concept behind the AI approach to continuous mapping.

FROM TENSOR TO GEOLOGY

The anomalous magnetic tensor is an abstract concept but is best imagined as a continuous change in curvature of the Earth's magnetic field. Direct measurement of the tensor in an airborne platform is now possible (Chwala et al., 2012; Stolz et al., 2017) and it can also be derived from a grid of the total magnetic intensity using Fourier transformation (Pratt et al., 2018).

Unlike TMI data, a single tensor measurement has inherent 3D properties that provide information about the geology on either side of the flight line. This insight leads us to the concept of using tensor line data to build a geological model that consists of one segment for each anomaly on every line in the survey (Figure 3).

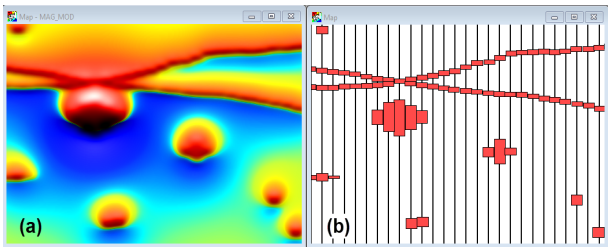

Figure 3. Colour image of the total magnetic intensity (a) and the segment model used to compute the response (b).

We explore here the geological properties that can be derived from the magnetic tensor without requiring inversion of one or more tensor measurements.

Important Tensor Properties

The magnetic gradient tensor is defined in Equation 1.

$$\Gamma = \begin{bmatrix} B_{xx} & B_{xy} & B_{xz} \\ B_{yx} & B_{yy} & B_{yz} \\ B_{zx} & B_{zy} & B_{zz} \end{bmatrix} = \begin{bmatrix} \frac{\partial B_x}{\partial x} & \frac{\partial B_x}{\partial y} & \frac{\partial B_x}{\partial z} \\ \frac{\partial B_y}{\partial x} & \frac{\partial B_y}{\partial y} & \frac{\partial B_y}{\partial z} \\ \frac{\partial B_z}{\partial x} & \frac{\partial B_z}{\partial y} & \frac{\partial B_z}{\partial z} \end{bmatrix} \quad (1)$$

Eigenvector decomposition of the symmetric tensor matrix produces a rotated and simplified version of the tensor ($\underline{\mathbf{\Lambda}}$) (Pedersen and Rasmussen, 1990; Clark, 2012).

$$\underline{\mathbf{\Lambda}} = \begin{bmatrix} \lambda_1 & 0 & 0 \\ 0 & \lambda_2 & 0 \\ 0 & 0 & \lambda_3 \end{bmatrix} \quad (2)$$

where $\lambda_1 > \lambda_2 > \lambda_3$ are the eigenvalues of the magnetic gradient tensor (Pedersen and Rasmussen, 1990; Clark, 2012). The three eigenvalues are found by solving the characteristic equation $\det(\underline{\mathbf{B}} - \underline{\mathbf{\Lambda}}\,\mathbf{I}) = 0$ while the three eigenvectors $\hat{\mathbf{e}}_1$, $\hat{\mathbf{e}}_2$, $\hat{\mathbf{e}}_3$ are found by solving the linear equation $\underline{\mathbf{B}}\,\hat{\mathbf{e}}_i = \lambda_i \hat{\mathbf{e}}_i$ where λ_i is the eigenvalue corresponding to $\hat{\mathbf{e}}_i$.

Pedersen and Rasmussen (1990) derive several parameters from the eigenvalues that are important for extracting useful geological characteristics from the target anomalies.

The rotational invariants I1 and I2 are defined as:

$$I_1 = B_{xx}\,B_{yy} + B_{yy}\,B_{zz} + B_{xx}B_{zz} - B_{xy}^2 - B_{yz}^2 - B_{xz}^2 \quad (3)$$

$$I_2 = B_{xx}\,(B_{yy}B_{zz} - B_{yz}^2) + B_{xy}\,(B_{yz}B_{xz} - B_{xy}B_{zz}) + B_{xz}\,(B_{xy}B_{yz} - B_{xz}B_{yy}) \quad (4)$$

The dimensionality index is defined as:

$$I = -\left(\frac{(I_2/2)^2}{(I_1/3)^3}\right) \quad (5)$$

This parameter is very important because it can tell us if the target is pipe-like (~1) or has extended strike (~0). It provides the AI engine with a numeric value that can separate pipes from dykes and a continuum in between. A pluton with an elliptic shape could have a I value of around 0.5 to 0.75. This one parameter helps provide important information for depth and magnetic susceptibility estimation.

If the dimensionality is low, then the source also has a strike or azimuth direction that can be computed from the tensor components (Pedersen and Rasmussen, 1990).

$$\tan(2\,\theta_s) = 2\,\frac{(B_{xy}(B_{xx}+B_{yy})+B_{xz}B_{yz})}{(B_{xx}^2-B_{zz}^2+B_{xz}^2-B_{yz}^2)} \quad (6)$$

where, θ_s is the strike direction of the longer axis of the magnetic source.

Parameters Derived from NSS

We calculate the dimensionality index and strike direction at the centre of magnetisation rather than as continuous functions. Clark (2012) further developed the concept of normalised source strength (NSS, μ), originally developed by

Wilson (1985) as an important new parameter that could be derived from the magnetic gradient tensor (Equation 7).

$$\mu = \sqrt{(-\lambda_2^2 - \lambda_1\lambda_3)} \text{ where } \lambda_1 > \lambda_2 > \lambda_3 \quad (7)$$

It has many special characteristics, because it is semi-independent of the source magnetisation direction. The NSS parameter peaks over the centre of magnetisation for discrete bodies and along the central axis of elongate sources. There is no need to perform a reduction to pole which is a great benefit at low field inclinations due to the instability of the RTP calculation. For wide sources, NSS peaks over the edge and for narrower targets the maximum gradient point of the NSS anomaly profile define the outer limits of the high magnetisation zone. If the depth-to-width ratio is less than 1, we cannot resolve the true location of the edge, but we can define its maximum possible lateral extent or a susceptibility-thickness product.

We use Nelson's formulation (Nelson, 1988) to compute an estimate for the apparent magnetic susceptibility;

$$k = 0.625\, z\, T_{g0}\, /(B_{IGRF}(\sin^2 I_f + \cos^2 D_f)), \quad (8)$$

where the total gradient

$$T_{g0} = \sqrt{B_{xx}^2 + B_{yy}^2 + B_{zz}^2} \quad (9)$$

and

z is the target depth below the sensor
B_{IGRF} is the inducing field strength
I_f is the magnetic field inclination
D_f is the magnetic field declination

A first order detection for remanence is determined by a sign reversal of the vertical gradient component B_{zz} or the first invariant I_1 at the centre of magnetisation.

Beike et al. (2012), Clark (2014) and McKenzie (2019) show that the inclination ϕ of the magnetisation of a compact source (including a dipole, sphere, ellipsoid and vertical pipe) can be calculated from the tensor measurement over the centre of magnetisation using the following formula:

$$\phi = \cos^{-1}\left(\frac{\lambda_2}{\mu}\right) - \pi/2 \quad (0 \leq \phi \leq \pi) \quad (10)$$

where λ_2 is the second eigenvalue and μ is the normalised source strength. The declination of the magnetisation may be estimated from the x and y components of the second eigenvector (McKenzie, 2019). Note that the magnetisation direction cannot be determined for extremely elongate magnetic sources.

From the magnetic tensor over the centre of magnetisation and the NSS profile, we recover many geological attributes for each target anomaly:

- Target style - pipe, elliptic pluton or dyke-like
- Strike direction for elongate targets
- Centre of magnetisation (origin)
- Apparent magnetic susceptibility
- Magnetic reversals
- Magnetisation inclination
- Target edges

The tensor and segment model concept provide a foundation for anomaly detection and analysis of the attributes of the magnetic anomaly source. A complete model of the geology requires enough segments to provide a suitable source for every anomaly on every line in the survey where the anomaly amplitude exceeds a predetermined threshold. When compared with a voxel model that covers the same footprint, it has the advantage of variable resolution for precision mapping of the geological boundaries, but also provides depth, compact physical property information, strike direction and some magnetisation information. The computational overhead for modelling is also reduced by several orders of magnitude compared with voxel model inversion at a similar resolution.

USING SOFT DATA WITH AI

All the parameters derived up to this point are considered hard facts that are based on geophysical theory and reproducible on any computer system. As interpreters, we use a lot of soft information as part of the process for converting geophysical data into a meaningful, geological/geophysical interpretation. We ultimately want to estimate the depth of each magnetic target and assess the quality of individual solutions that might be compromised by interference or limitations in the geophysical model. Importantly, we must derive a satisfactory segment solution for every anomaly on every line above a predetermined anomaly threshold.

We analyse both sides of every NSS anomaly (Figure 4) and collect information such as:

- Peak and trough locations
- Inflection point locations
- Curvature point locations
- Interference
- Characteristic amplitudes
- Characteristic widths
- Characteristic ratios

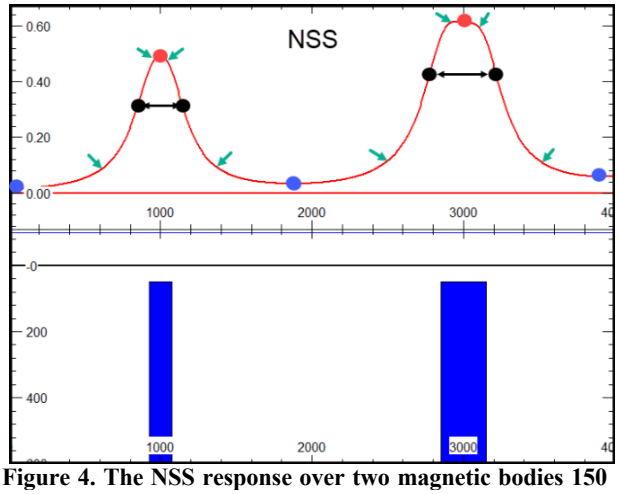

Figure 4. The NSS response over two magnetic bodies 150 m below the sensor and widths of 150 and 300 m. The field inclination is -60 degrees and declination 10 degrees north. The peaks (red dots), troughs (blue dots), inflection points (black dots) and curvature points (green arrows) represent the characteristic points on the NSS curve.

The ratio of depth to width is an important factor for improving the quality of depth interpretation and as part of the training of the AI system we have developed a suite of tests to detect ratios in the range 1.0 < DW < 2.0 where DW is the depth-to-width ratio. When DW is greater than 2.0, we use

shape characteristics that are equivalent to the anomaly over a body edge. The width classification information is also used to correct the initial body width which is based on the location of the inflection points.

The inflection and curvature points of the NSS anomaly curve form the foundation for the estimation of an initial depth value. This initial value is then corrected based on the depth to width classification and strike azimuth relative to the line direction. The strike azimuth correction is only applied to low dimensionality (I) anomalies.

Working with Complex Geology

The AI system is designed to interpret every anomaly but, this is a difficult task. Isolated anomalies will produce much better physical property and depth estimates than those that are overlapping. We call this interference and it turns out that the normalised source strength parameter has excellent properties for detection and estimation of interference. The base level for the NSS curve is zero, therefore there is little or no regional present unless there is a high magnetic susceptibility unit at depth below the target anomaly. We use the amplitude of the low on either side of the target as a relative indicator of the amount of interference. Figure 5 shows increasing levels of interference (green arrows, middle track) as the edge of one magnetic source approaches its neighbour. The NSS curve is symmetric about the body centre compared with the vertical magnetic gradient (B_{zz}). Note that peaks separate as the width increase beyond twice the depth below the sensor.

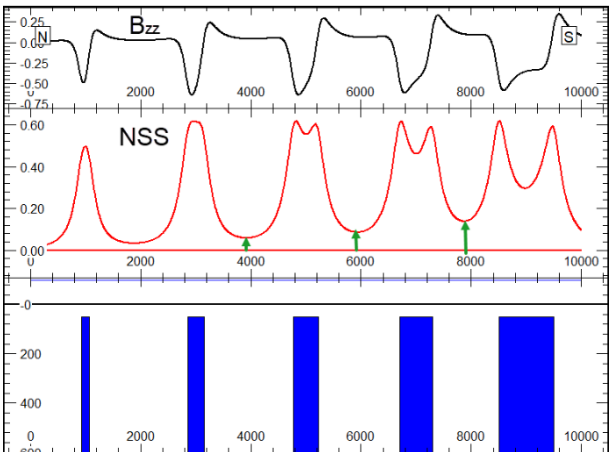

Figure 5. This model simulation of a series of increasing width bodies illustrates the impact of edge proximity on the amplitude of the trough between adjacent magnetic sources. The field inclination is -60 degrees and declination 10 degrees north.

We have developed an anomaly classification scheme that uses the following anomaly characteristics:

- Discrete – isolated narrow anomaly (DW <= 1.0)
- Discrete medium – isolated anomaly (1.0 > DW < 2)
- Wide – left or right side of a wide body (DW >= 2)
- Group – left or right edge of an anomaly group
- Group internal – interfering anomalies on both sides

Curvature parameters and interference were both used as input for training the classification algorithm. Figure 6 shows an example plot of curvature ratios produced by a training run on a synthetic geological model. The different colours show the anomaly type classification.

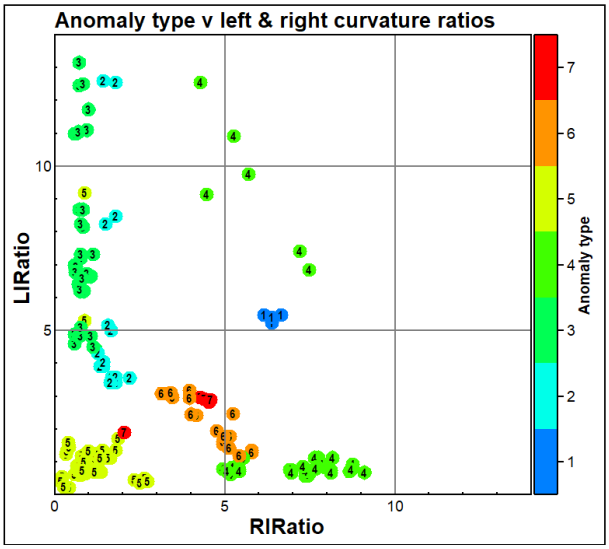

Figure 6. A cross-plot of the left and right curvature ratios from a synthetic geological model. The anomaly classes are colour coded by their class number.

False positives are generated by lines that pass near to a magnetic source, but not over it. The tensor helps eliminate these anomalies from the analysis by computing the ratio of the total horizontal gradient to the vertical gradient at the NSS peak. When the horizontal gradient dominates, the sensor is generally not over the magnetic source. This simple parameter eliminates many but not all, false picks.

Depth Estimation and Correction

A preliminary depth estimate is computed for each side of the NSS profile using the characteristic curvature. A strike correction is applied first to the depth estimate and then the AI system uses input from the dimensionality index (I), segment width, anomaly type classification and interference to correct the depth using the training information determined from trial geological models. The magnetic susceptibility estimate is then calculated using the depth and total gradient data (Equations 8 and 9) and refined using the training information.

MODEL TESTS

Many model surveys were simulated over varying geological models to provide both insights into parameter sensitivity and training data for calibration of the AI system.

Figure 7 shows a plot of isolated tabular models with finite strike length, variable orientation and variable magnetic susceptibilities designed to test the azimuth calculations. Azimuth-oriented, coloured segments are posted over the original models (black outline) that were used to generate the magnetic tensor data. The symbols are colour coded by the estimated segment depth with azimuth annotations beside the symbols. If the end segments are excluded, the azimuth results are all within 1 to 2 degrees of the model orientations. Different logic is required to recognise and manage the end members of a string of segments. Work on this logic is part of a parallel research project that chains segments together from adjacent lines for use in the assessment of property variance along the chain.

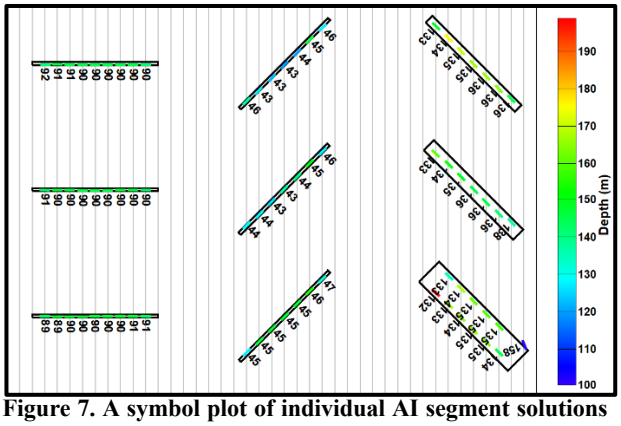

Figure 7. A symbol plot of individual AI segment solutions using the azimuth to control symbol rotation and depth to modulate colour. The symbols are posted over outlines of the original bodies at 150 m depth and the annotations show the computed azimuth value. The two left-hand columns of bodies have susceptibilities from top to bottom of 0.005, 0.05, 0.5 SI units. The right-hand column of bodies all has susceptibilities of 0.05 SI.

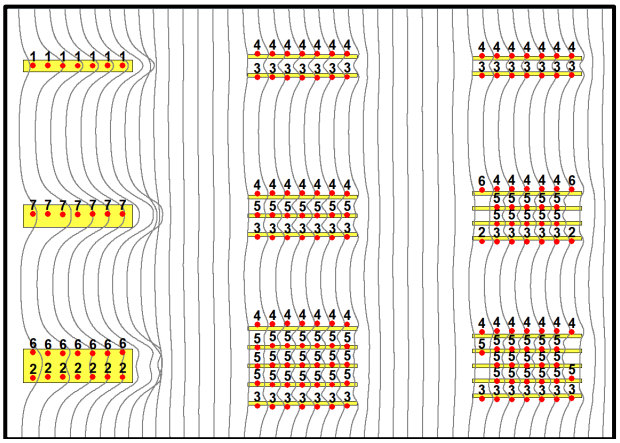

Figure 8. An example of tabular bodies with varying thickness or varying spacings with a stacked profile map of the NSS model. The numbers posted beside the segment centres are the AI determined segment classifications based on its location relative to the geological feature.

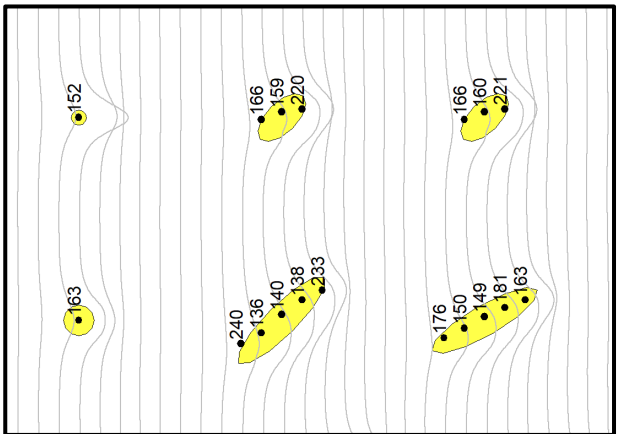

Figure 9. A stacked profile map of the NSS parameter posted over the original pipe models and AI derived segments (black dot locations) with individually computed depth estimates.

One of the limitations of any automated magnetic interpretation system is the ability to differentiate between geological shapes and understand what level of quality can be assigned to an individual solution. Much of our testing focused on understanding the behaviour of the AI system in the presence of interfering sources and edge effects. Every discrete magnetic zone will produce a magnetic anomaly, but many are not suitable for depth or physical property calculations. We need to account for them so that ultimately, they can be included in a full model inversion. When strong interference is present, computed depths will usually appear shallower due to the shortening of the anomaly between adjacent magnetic sources. However, if we know that one edge of the anomaly is also the edge of a group, then that edge can provide a more robust depth estimate. Figure 8 provides an illustration of individual segment classifications based on the anomaly style.

While there is a strong impression of coherence in the distribution of segments, they have been located on an individual basis with no knowledge of segments on adjacent flight lines. An example of the effect can be seen in Figure 9 which shows the depth results for a series of circular and elliptic shaped intrusive pipes, all at a depth of 150 metres below the sensor. The central segments for each pipe are within 10 metres of the true depth but, for the elongate pipes, the depths deteriorate towards the ends due to the longer anomaly wavelengths near the ends. This decrease in accuracy can be ameliorated by using AI principles or inversion.

LIMITATIONS

While the AI system helps to produce robust outcomes and aims to produce realistic results in a broad range of geological scenarios, the primary constraint is the assumption of an unconformity that cuts steeply dipping basement rocks. This model fits a broad range of geological problems in exploration mapping, but it does not fit all possible situations. Interpreters must make their own decisions on the suitability of this model for their own study.

Depth is one of the most important parameters to be derived by this AI methodology, but the precision is limited by factors such as depth-to-width ratio, interference and precision of the tensor data. There are also limitations associated with proximity to the end of a segment group.

The magnetisation direction can be computed for compact sources such as intrusive pipes and ellipsoid style targets but, further investigation is required to test the credibility of the results over large areas. This is a high priority for further research because it has the potential to expose a range of target styles that are often lost in conventional magnetic data analysis (Pratt, 2013; Pratt et al 2014).

In the case of conventional surveys, the tensor is calculated from the TMI grid. If the flight lines are widely spaced relative to the flying height, then the quality of the tensor is reduced. The quality can be improved by upward continuation, but this also reduces the precision of the depth estimates.

While the tensor reduces the impact of regional factors, it can still impact on the depth quality in the vicinity of high magnetic susceptibility intrusions beneath the unconformity.

CASE HISTORY

The AI system was applied to a recent data subset from the South Australian PACE Copper program over the Gawler Craton, Torrens sheet (Figure 10). The total field magnetic and radiometric survey was flown in 2017 at 200 metre line spacing and 60 metre terrain clearance by Sander Geophysics Limited (Bates and Dennis, 2018). A geophysical report on the image processing and depth interpretation of the survey results is presented by Foss et al. (2018).

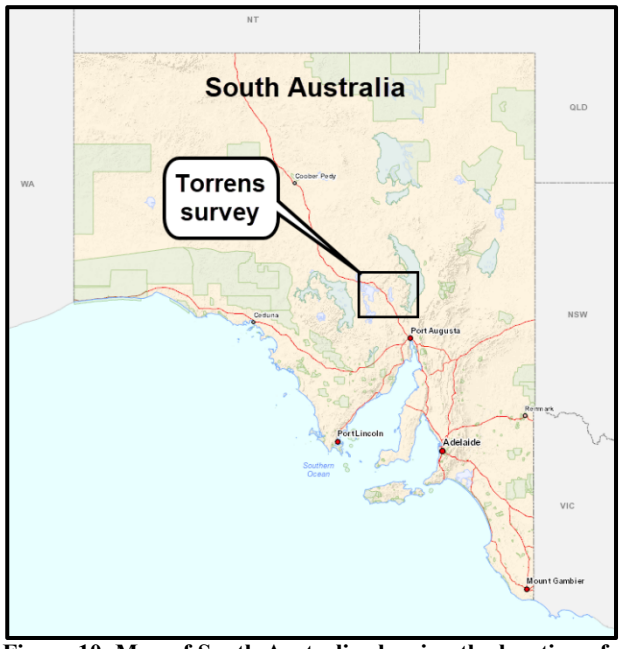

Figure 10. Map of South Australia showing the location of the Torrens aeromagnetic survey.

The total magnetic intensity image for the Torrens survey area is shown in Figure 11. The north-west trending Gairdner Dyke swarm disturb the high amplitude anomalies associated with the deeper magnetic basement.

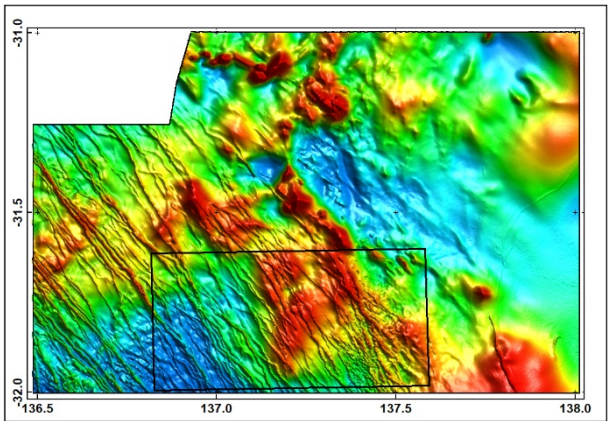

Figure 11. A total magnetic intensity image of the total magnetic intensity grid supplied by the South Australian Geological Survey. The black rectangle shows the location of data used in the case history.

The magnetic tensor data was computed by FFT transformation of the TMI data using ModelVision (Pratt et al., 2018). The grid data was then resampled back on to the original flight lines in preparation for the AI processing. A subset of the Torrens tensor data, reduction to pole (RTP), first vertical derivative (BmVD) and normalised source strength images is shown in Figure 12. Note that the BmVD and RTP channels are not required for the processing but are shown for comparison with the tensor channels.

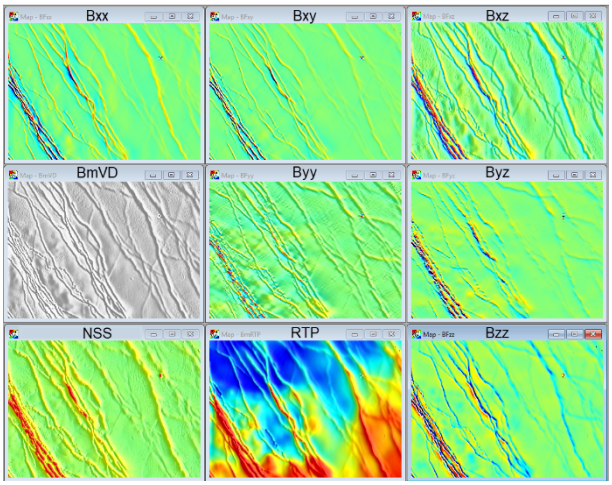

Figure 12. A matrix image of the tensor channels (6 upper right squares). The first vertical derivative, normalised source strength and reduction to pole channels are shown in the lower left segments.

A detailed pseudo-colour image of the TMI case history study area is shown in Figure 13. Figure 14 presents some of the interpreted attributes after the AI processing of a subset of the study area results, overlain on a monochrome image of the total magnetic intensity. Approximately 50 attributes have been computed by the AI system at this stage of processing and a proportion of them are suitable for display as symbols with attributes such as size, colour, azimuth and text. In Figure 14 we have chosen to use black dots where the size is modulated by the AI system estimate of depth confidence. The text annotation is used for the estimated depth below the ground surface. Beneath the symbol, a model representation of the upper surface of each segment is shown and colour coded by the magnetic susceptibility.

At this point in the process, the segments have been generated independently of segments from adjacent lines but, the process demonstrates that there is considerable coherence in the spatial relationships. The model segments have a strike direction that was derived directly from the tensor (Equation 6) and are colour coded by the estimated magnetic susceptibility (Equation 8). The depth confidence (black dot size) provides a useful guide on which depths to use during interpretation.

These preliminary results suggest the existence of four unconformity surfaces:

- Sub-crop or surficial 0 to ~50 metres, generally lack spatial coherence
- Gairdner Dykes 50 to 100 metres, low susceptibility
- Gairdner Dykes 100 to 200 metres
- Basement >250 - 300 metres (not shown here)

Figure 15 shows the model segments for the whole study area overlain on a monochrome image of the total magnetic intensity grid, but without the depth annotations. The coherence of the individual azimuth-oriented model segments is evident and enhances the interpreter's ability to absorb the underlying geological information.

Figure 16 shows one of many possible display styles where attributes are used to modulate the size and colour of filled circles. In this case, the colour represents magnetic susceptibility and the size is controlled by the susceptibility-thickness product. Since it is not possible to estimate the thickness of the dykes, the susceptibility-thickness product becomes a useful diagnostic parameter. Other parameters include width, magnetisation inclination, magnetisation declination, apparent magnetisation departure angle, anomaly reversal, pipe classification, dimensionality, anomaly amplitude, interference and many others.

CONCLUSIONS

We have demonstrated that is possible to use the inherent 3D information in the magnetic gradient tensor along with the higher resolution of flight line data to build a 3D magnetic model of one or more unconformity surfaces. The problem is simplified by using a single segment for every anomaly in every line in the survey where the segment strike length is equal to the line spacing.

The AI expert system plays an important role by applying geological principles to the assessment and refinement of every segment in the survey. The additional information produced by the AI system provides the interpreter with important shape, property and quality attributes which make the process of interpretation more robust. We believe that neural network AI methods also have a role to play for improving some of the classification parameters that are used by the expert system.

The AI process assumes that all anomalies are truncated by an unconformity surface which is a practical assumption for many airborne surveys. It does not attempt to consider continuous property variations except at the scale of the flight line spacing.

This research is the first stage of a multi-stage AI process designed to produce coherent, quantifiable 3D magnetic lithology models at a resolution that reflects the detail present in the original survey. These results provide the foundation for exploring the links between adjacent segments, lateral continuity along segment chains, equivalent source joint inversion of the magnetic gradient tensor, micro-adjustment of individual segments based on joint inversion and magnetisation property recovery through inversion.

ACKNOWLEDGEMENTS

We would like to acknowledge the input of Anglo Operations and De Beers for their encouragement and partial support for the development of a new way of interpreting full tensor magnetic data.

REFERENCES

Bates,M., and Dennis, J., 2018, PACE Gawler Craton Airborne Geophysical Survey Program: Block 3B – Torrens, SGL Technical Report (unpublished) 218p.

Beike, M., Clark, D.A., Austin, J.R. and Foss, C.A. 2012, Estimating source location using normalized magnetic source strength calculated from magnetic gradient tensor data: Geophysics, 77, (6), J23-J37.

Chwala, A., Stolz, R., Zakosarenko, V., Fritzsch, L., Schultz, M., Rompel, A., Polome, L., Meyer, M. and Meyer, H.G. 2012, Full Tensor SQUID Gradiometer for airborne exploration. Extended Abstracts, 22nd International Geophysical Conference and Exhibition, 26-29 February 2012 - Brisbane, Australia.

Clark, D.A., 2012, New methods for interpretation of magnetic vector and gradient tensor data I: eigenvector analysis and the normalised source strength: Exploration Geophysics, 43, 267-282.

Foss, C.A., Gouthas, G., Fabris, A., Werner, M., Katona, L., Hutchens, M. and Reed, G. 2018, Gawler Craton Airborne Geophysical Survey Region 3B, Torrens – Enhanced geophysical imagery and magnetic source depth models. Report Book 2018/00038, Government of South Australia, 76p.

McKenzie, K.B., 2019, The magnetic tensor of a triaxial ellipsoid, its derivation and its application to the determination of magnetisation direction (Exploration Geophysics, in press).

Pedersen, L.B. and Rasmussen, T.M., 1990, The gradient tensor of potential field anomalies: Geophysics, 55 (12), 1558-1566.

Pratt, D.A., McKenzie, K.B., White, A.S., Foss, C.A., Shamin, A. and Shi, Z. 2001, A User Guided Expert System Approach to 3D Interpretation of Magnetic Anomalies. Extended Abstracts, ASEG 15th Geophysical Conference and Exhibition, August 2001, Brisbane.

Pratt, D.A., 2013, The potential of remote remanence estimation (RRE) for kimberlite exploration – A case history from the Thomson Fold Belt. Extended Abstracts, 23rd International Geophysical Conference and Exhibition, 11-14 August 2013 - Melbourne, Australia.

Pratt, D.A., McKenzie, K.B. and White, A.S., 2014, Remote remanence estimation (RRE). Exploration Geophysics, 45(4), 314-323.

Pratt, D.A., Parfrey, K., White, A.S. and McKenzie, K.B. 2018, ModelVision v16.0 User Guide, pub. Tensor Research, 599p.

Pratt, D.A., McKenzie, K.B. and White, A.S., 2019, An AI approach to using magnetic gradient tensor analysis for quick depth and property estimation. Extended Abstracts, AEGC 2019: From Data to Discovery – Perth, Australia.

Stolz, R., Zakisarenko,V., Schmelz, M., Schiffler, M., Chwala, A., Meyer, M. and Meyer, H.G. 2017, SQUIDs in exploration: the past, present and future. Extended Abstracts - 15th SAGA Biennial Conference and Exhibition.

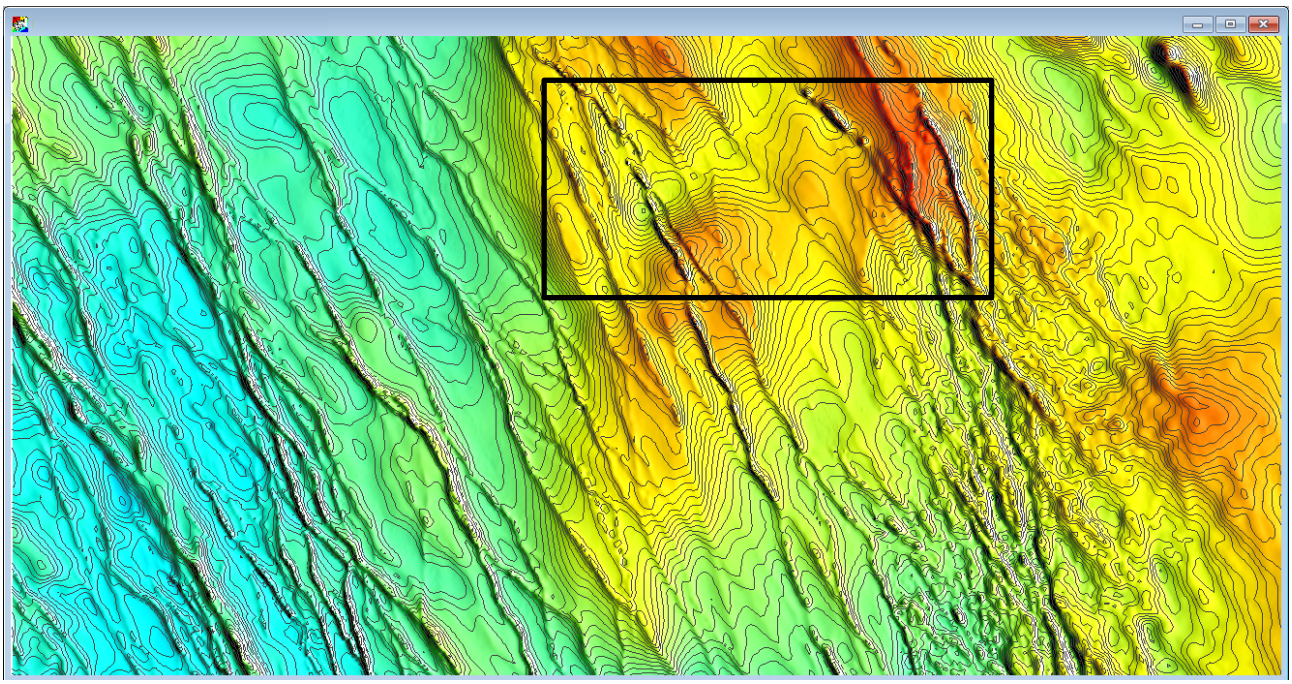

Figure 13. A pseudo-colour image of the total magnetic intensity grid for the area covered by the case history study. The black rectangle represents the location of the selected subset used in Figure 13(b).

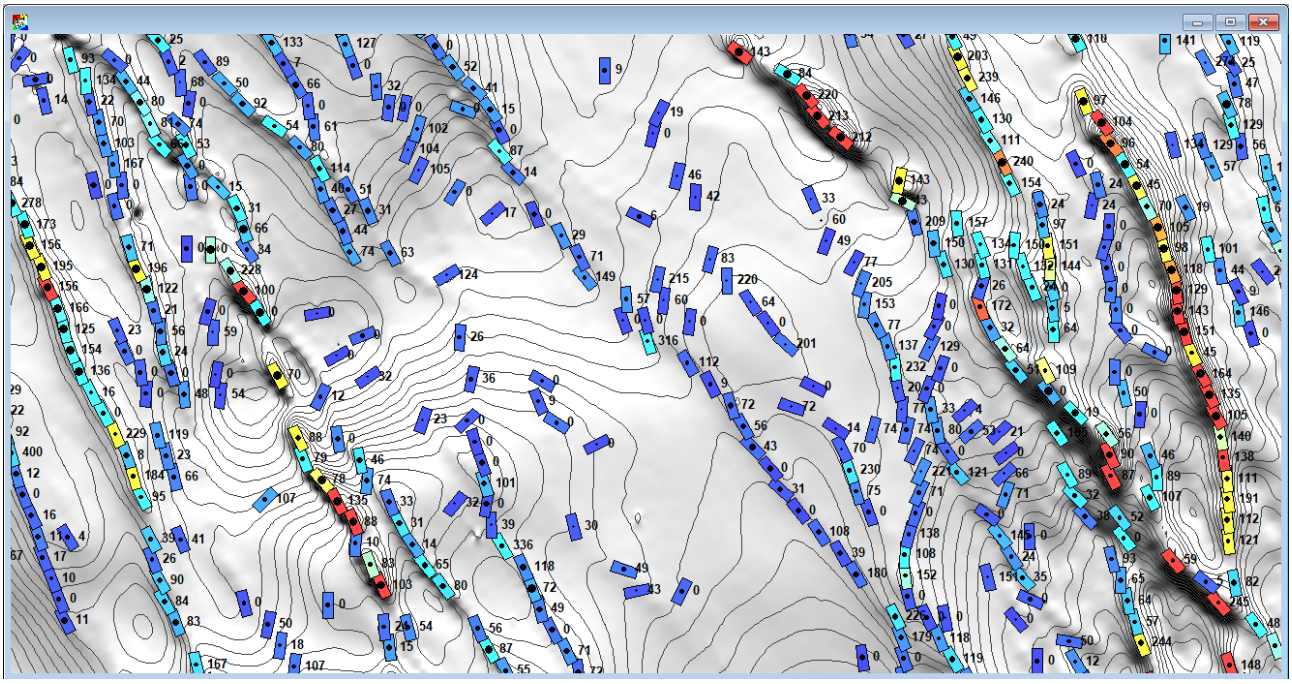

Figure 14. A subset of the study area posted over a monochrome image and contours of the total magnetic intensity grid. Individual segment models were derived from the anomaly attributes and are oriented according to the tensor-derived azimuth and colour coded by magnetic susceptibility. The depth annotations show depth (m) below the ground surface and the associated black dot varies in size according to the AI assessment of depth quality.

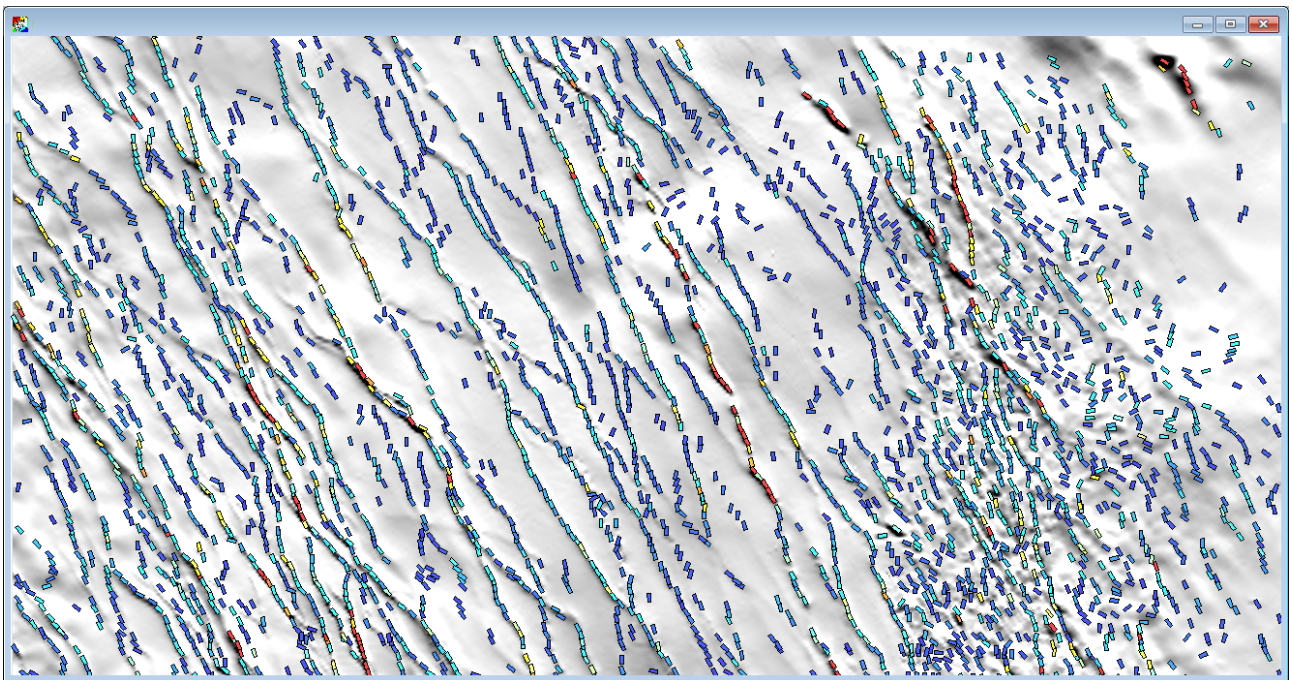

Figure 15. Model segments for the complete study area are posted over a monochrome image of the total magnetic intensity grid. Individual segment models were derived from the anomaly attributes and are oriented according to the tensor-derived azimuth and colour coded by magnetic susceptibility. The visual coherence of individually derived segments is enhanced by using the tensor-derived azimuth.

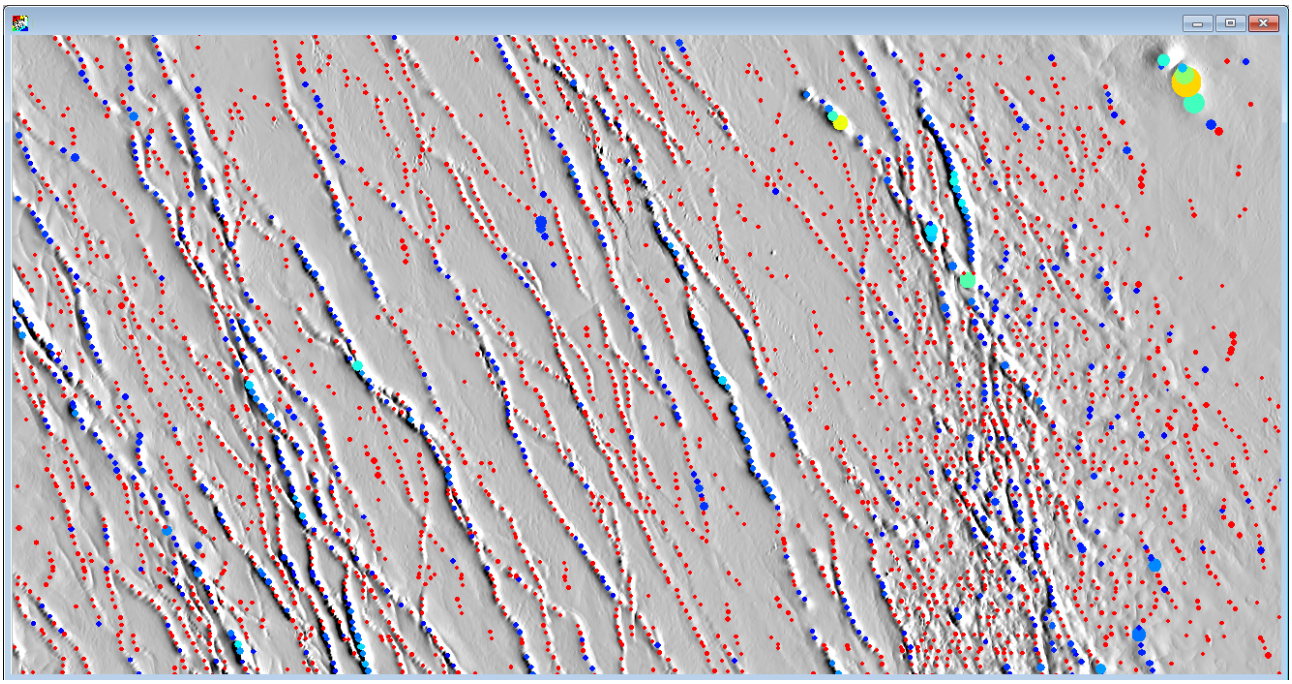

Figure 16. Coloured symbols represent attributes for individual anomalies posted over an image of the normalised source strength. The colour is modulated by magnetic susceptibility from blue (low) to high (red) and the symbol size is modulated by the susceptibility-thickness product. The large symbols in the upper right corner are associated with the basement rocks.